Materials Letters 305 (2021) 130789

Contents lists available at ScienceDirect

Materials Letters

journal homepage: www.elsevier.com/locate/matlet

Phase stability of novel HfNbTaTiVZr refractory high entropy alloy under ion irradiation

Jianren Zhou [a,*], Mark Kirk [b], Pete Baldo [b], Shengmin Guo [a], Fengyuan Lu [a]

[a] Department of Mechanical and Industrial Engineering, Louisiana State University, Baton Rouge, LA 70803, USA
[b] Division of Nuclear Engineering, Argonne National Laboratory, Lemont, IL 60439, USA

ARTICLE INFO

Keywords:
HfNbTaTiVZr
Refractory high entropy alloy
Phase stability
Ion irradiation

ABSTRACT

HfNbTaTiVZr refractory high entropy alloy (RHEA) fabricated by arc melting shows the single-phase body-centered cubic (BCC) structure. Radiation-induced amorphization (RIA) is observed at 2 displacements per atom (dpa) at 298 K while the specimen remains its crystal structure at 423 K. The critical amorphization temperature (T_c) is likely within 298–423 K. RIA is mainly attributed to the accumulation of Frenkel pairs caused by elastic collisions under ion irradiation and the large atomic size mismatch in the studied RHEA facilitates the amorphization process. RIA of RHEA is for the first time reported and the finding challenges the current understanding of phase stability of RHEAs upon irradiation.

1. Introduction

RHEAs have been proposed to be the new generation of structural materials due to the novel alloy design, high strength, wear [1], corrosion [2] and radiation resistance [3]. RHEAs with BCC structures are considered as promising candidates for high temperature applications in advanced nuclear reactors due to the high melting temperature and enhanced strength at elevated temperature. RHEAs are also likely to have good radiation-induced swelling and creep resistance [4]. However, it requires comprehensive evaluations of material properties for their actual service in reactors because of the extreme conditions like high temperature, high radiation damage and complex corrosive environment. Studies [3,4] show good radiation resistance of BCC HEAs, however, the mechanisms that affect the radiation tolerance are still elusive. This work investigates phase stability of novel HfNbTaTiVZr RHEA under 1 MeV Kr^{2+} ion irradiation at 298 and 423 K and discusses the relation between alloy parameters and phase stability. This study reveals a large atomic size mismatch in RHEA may favor amorphization under irradiation and this finding offers a critical down-selection of potential candidates.

2. Material and methods

The HfNbTaTiVZr RHEA was fabricated using a vacuum arc melting furnace (Edmund Buhler/ MAM-1) under argon atmosphere in a water-cooled copper hearth. Powders with high purity were mixed for 15 min and pressed at 350 MPa to obtain the green body. The green body was then melted using the arc melter for 4 times to ensure the homogeneity of the composition and microstructure. The synthesis process was discussed in detail by Gao et al. [5]. The crystal structure of the as-casted alloy was characterized by XRD (Empyrean, PANalytical) with the 2θ scan varying from 20° to 100° at a scan speed of 0.05°/s and an accelerating voltage of 45 kV and current of 40 mA. The TEM specimens were prepared by a "lift-out" method using focused ion beam (FIB) system with Ga^+ ions (FEI, Quanta 3D FEG). *Ex situ* transmission electron microscopy (TEM) techniques were used to characterize the specimens using a JOEL 2010 TEM facility (operating at 200 kV) at the shared instrument facility of Louisiana State University.

Phase stability of HfNbTaTiVZr RHEA under 1 MeV Kr^{2+} ion irradiation was investigated using Intermediate Voltage Electron Microscopy (IVEM)-Tandem facility at Argonne National Laboratory. The IVEM-Tandem facility was equipped with a Hitachi H-9000NAR TEM (operating at 200 kV) interfaced to a 650 KV NEC ion accelerator and ion implanter (ion flux of $6.25X10^{11}$ ions cm^{-2} S^{-1}). This flux rate gives an efficiently high rate of irradiation while minimizing specimen heating. Krypton was chosen due to its inert chemical properties to the irradiated material and its ability to produce high damage dose in a relatively short time. The ion beam was oriented to the microscope axis at an angle of 30° and homogeneous over an area of 1.5 mm in diameter. The specimens were tilted between 5° and 20° from the electron beam to irradiate

* Corresponding author.
E-mail address: CarlChow89@gmail.com (J. Zhou).

https://doi.org/10.1016/j.matlet.2021.130789
Received 29 July 2021; Received in revised form 16 August 2021; Accepted 27 August 2021
Available online 2 September 2021

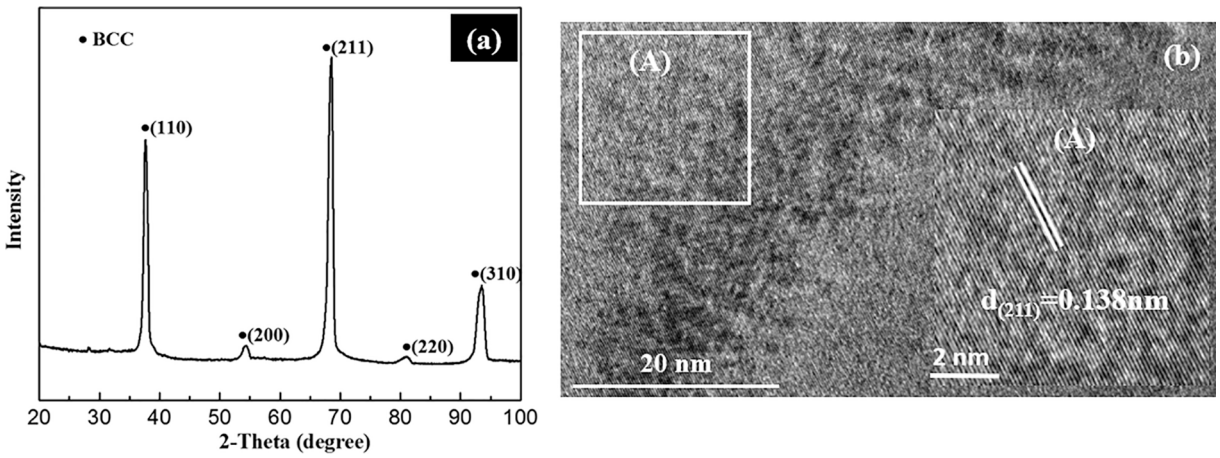

Fig. 1. Structure of HfNbTaTiVZr RHEA: (a) XRD pattern and (b) high-resolution TEM image. The IFFT image is inserted as (A).

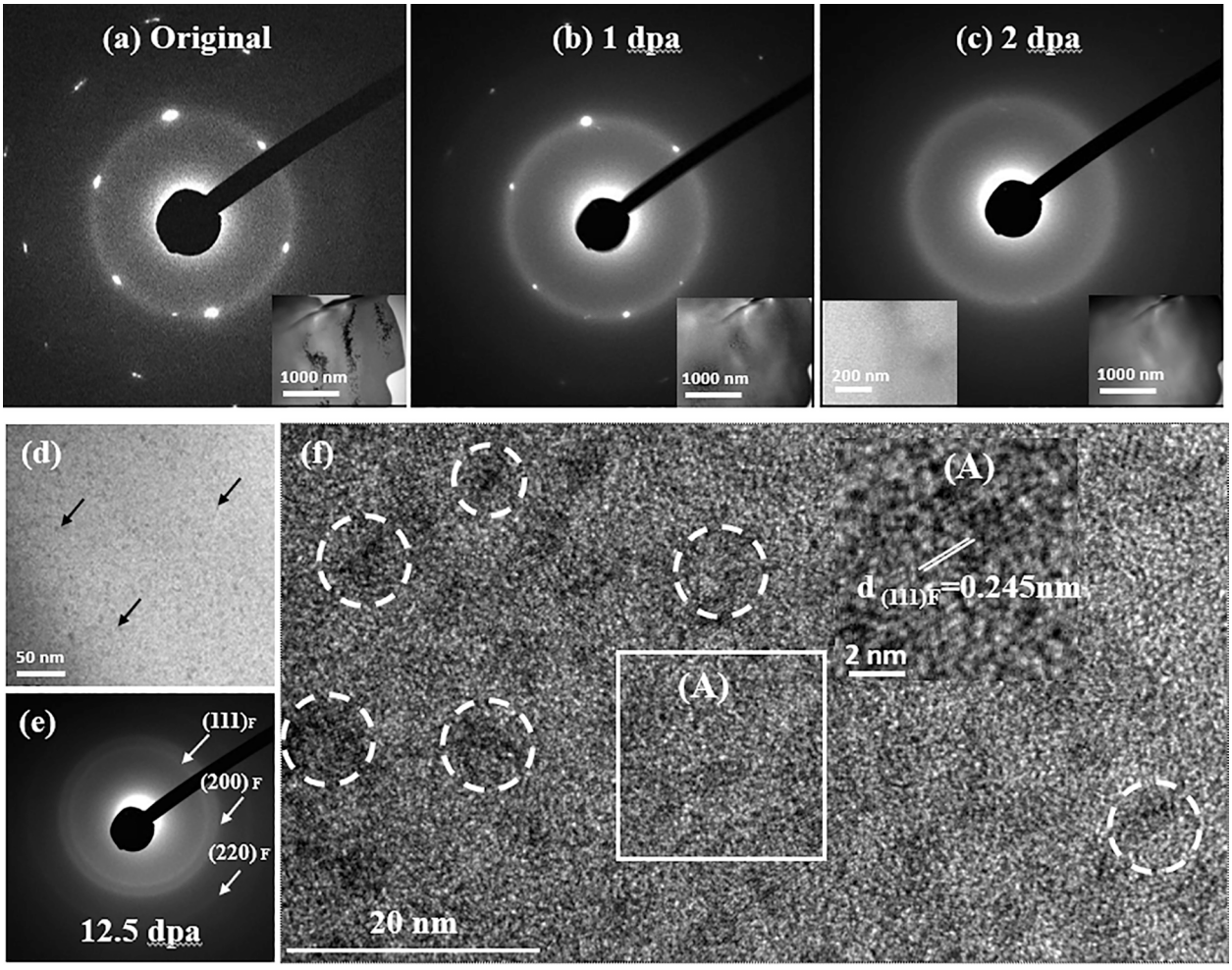

Fig. 2. Series of TEM BF images, DF image (inserted), and SAD patterns of HfNbTaTiVZr RHEA irradiated at 298 K, (a) unirradiated, (b) 1 dpa (4×10^{14} ion/cm^2), (c) 2 dpa (8×10^{14} ion/cm^2), (d) 12.5 dpa (5×10^{15} ion/cm^2), (e) SAD pattern at 12.5 dpa, (f) high-resolution TEM image at 12.5 dpa. The black arrows at (d) indicate radiation-induced precipitation.

the specimens simultaneously. *In situ* TEM techniques like bright field (BF), dark field (DF) and selected area diffraction (SAD) patterns were used to observe the radiation damage. Critical amorphous fluence was defined by the disappearance of all the diffraction intensities in the SAD pattern and was converted into the critical amorphization dose in the unit of dpa using Monte Carlo SRIM-2008 software with atomic displacement energy of 40 eV for each element[6].

3. Results and discussion

Fig. 1 (a) exhibits the XRD pattern of the as-casted alloy. All the major diffraction peaks are identified to belonging to a single-phase BCC

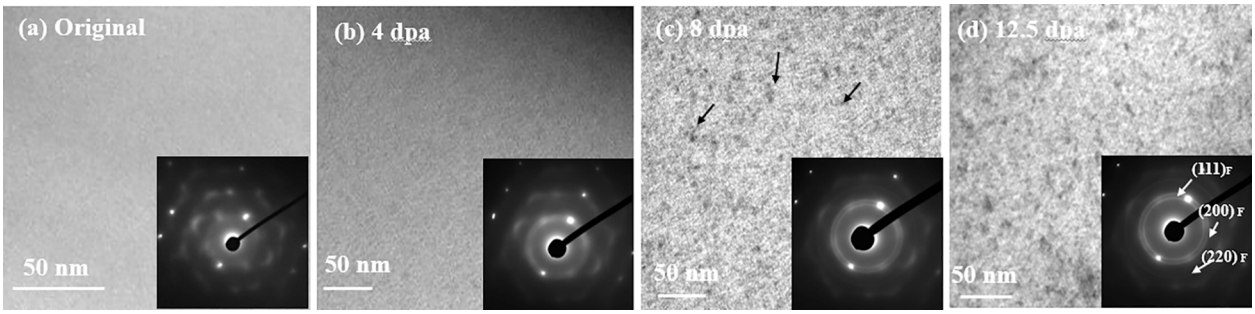

Fig. 3. Consequence of TEM BF images and SAD patterns of HfNbTaTiVZr RHEA irradiated up to 12.5 dpa at 423 K, (a) unirradiated, (b) 4 dpa (1.6×10^{15} ion/cm^2), (c) 8 dpa (3.2×10^{15} ion/cm^2), (d) 12.5 dpa (5×10^{15} ion/cm^2). The black arrows at (c) indicate radiation-induced precipitation.

structure. The lattice parameter of this BCC structure is determined as 0.334 nm that agrees well with the estimated value of 0.32 nm using the Vegard's law. Fig. 1 (b) shows the high-resolution TEM image with an orientation of (211).

Fig. 2 shows the crystalline to amorphous (c/a) phase transformation process at 298 K. A polycrystal structure is shown in Fig. 2 (a), where the BF image has a sharp contrast, and the SAD pattern is full of diffraction spots. BF image loses part of its contrast and the diffraction spots tend to form amorphous halos with the irradiation dose increasing to 1 dpa (4×10^{14} ion/cm^2) (Fig. 2 (b)). The crystalline phase totally transforms to amorphous state at an irradiation dose of 2 dpa (8×10^{14} ion/cm^2), denoted by the complete missing of the sharp contrast in the BF and DF images and the complete replacement of the diffraction spots by the halos in the SAD pattern (as shown in Fig. 2 (c)). Fig. 2 (d) shows the radiation-induced precipitation at 12.5 dpa in the amorphous phase, denoting by the nano-crystalline contrast and the appearance of the Debye rings in the corresponding SAD pattern in Fig. 2 (e). Fig. 2 (f) exhibits the high-resolution TEM image showing the structure of the precipitates with an average grain size of 5.5 nm. Fig. 3 shows the irradiation process at 423 K up to a dose of 12.5 dpa that the crystal structure is remained, and no phase transformation is observed. However, precipitation is observed at 8 dpa and grain growth of precipitate is seen with continuous irradiation. The final grains at 12.5 dpa have an average grain size of 9.7 nm. Electron diffraction shows the precipitates to be consistent with the face centered cubic, Ti-rich phase.

Atomic displacement cascades caused by the elastic collisions facilitate the movement of the displaced atoms, leaving radiation-induced point defects within the material. Ti is easier to be displaced from the lattice due to the lower displacement energy (19 eV) than the other elements [7], which introduces the Ti vacancies and interstitials in the lattice structure. At 298 K, the Ti vacancies and interstitials tend to form Frenkel pairs due to the limited atomic mobility and defect recombination rate. Amorphization occurs when the Frenkel defect reaches the critical concentration. On the other hand, the displaced Ti atoms will be dragged by mobile point defect fluxes towards defect sinks, causing solution-rich Ti clusters that induces precipitation under ion irradiation. But RIA is rarely observed in other HEAs and the amorphization in this studied RHEA can be associated with the large atomic size mismatch that produces strong atomic-level stress (strain) and local lattice distortion (LLD) lowering the threshold for amorphization [8]. The atomic size mismatch (δ) is defined as

$$\delta = \sqrt{\sum_{i=1}^{n} c_i \left(1 - r_i / \sum_{j=1}^{n} c_j r_j\right)^2} \quad (1)$$

where c_i and r_i are the atomic fraction and atomic radius of element i, and n is the total number of constituent elements. It is notable that a high LLD and atomic level stress (strain) maybe caused by the large δ of HfNbTaTiVZr RHEA. The mean squared displacement (U_{iso})in HfNbTaTiVZr RHEA is defined in equation (2), where DWF is Debye-Waller factor.

$$DWF = \exp(-Q^2 U_{iso}/3) \quad (2)$$

U_{iso} is calculated to be 0.1265 Å^2 that is extraordinarily larger than other RHEAs [9], indicating the existence of large LLD. For RHEA with Hf and Zr elements, the energy related to LLD is exceptionally large that will destabilize the phase stability under irradiation. The large LLD in HfNbTaTiVZr RHEA is also associated with the local atomic chemistry and the LLD is larger because of more extensive charge transfer that involves atoms in the first as well as second atomic shells [9]. Moreover, δ building up in the lattice increases the atomic level strain [10]. A high atomic level strain tends to make the lattice unstable and favors an amorphous state by releasing its strain energy under irradiation [11]. High atomic level stress (strain) also facilitates amorphization upon ion irradiation in a way like local thermal melting, as reported in [4,12]. Additionally, the high distortion and strain energy increase the free energy of the system that may lower the energy difference between crystalline and amorphous state, facilitating radiation-induced amorphization process. No amorphization is observed at 423 K that is related to a higher defect annealing ability at elevated temperature. Finally, HfNbTaTiVZr RHEA exhibits a better radiation tolerance than intermetallic compounds that can be amorphized at 0.1–0.5 dpa at 298 K [13]. This better radiation tolerance is attributed to a "self-healing" ability [4]. Radiation tolerance of RHEA has a strong relation with the LLD caused by atomic size mismatch and chemistry.

4. Conclusions

The HfNbTaTiVZr RHEA fabricated by arc melting exhibited a BCC structure. Radiation investigation under 1 MeV Kr^{2+} ions showed the alloy can be amorphized at 2 dpa at 298 K and the critical temperature is likely within 298–423 K. The large distortion and atomic level strain energy caused by large atomic size mismatch increase the system free energy that may lower the energy difference between crystalline and amorphous state, facilitating the amorphization. HfNbTaTiVZr RHEA possessed a better radiation tolerance than conventional nuclear materials due to a "self-healing" ability.

CRediT authorship contribution statement

Jianren Zhou: Writing – original draft, Writing - review & editing, Investigation. **Mark Kirk:** Investigation. **Pete Baldo:** Investigation. **Shengmin Guo:** Writing - review & editing, Funding acquisition. **Fengyuan Lu:** Supervision, Writing - review & editing, Funding acquisition.

Declaration of Competing Interest

The authors declare that they have no known competing financial interests or personal relationships that could have appeared to influence the work reported in this paper.

Acknowledgments

The work was supported by U.S. NRC-38-10-933, NSF OIA-1541079 and NSF OIA-1946231.

References

[1] N.B. Hua, W.J. Wang, Q.T. Wang, Y.X. Ye, S.H. Lin, L. Zhang, Q.H. Guo, J. Brechtl, P.K. Liaw, J. Alloy. Compd. 861 (2021), 157997.
[2] A. Parakh, M. Vaidya, N. Kumar, R. Chetty, B.S. Murty, J. Alloy. Compd. 863 (2021), 158056.
[3] D. Patel, M.D. Richardson, B. Jim, S. Akhmadaliev, R. Goodall, A.S. Gandy, J. Nuclear Mater. 531 (2020), 152005.
[4] T. Egami, W. Guo, P.D. Rack, T. Nagase, Metall. Mater. Trans. A-Phys. Metall. Mater. Sci. 45A (1) (2014) 180–183.
[5] M.C. Gao, B. Zhang, S. Yang, S.M. Guo, Metall. Mater. Trans. A-Phys. Metall. Mater. Sci. 47A (7) (2016) 3333–3345.
[6] P.H. Lei, G. Ran, C.W. Liu, C. Ye, D. Lv, J.X. Lin, Y.Z. Wu, J.K. Xu, Materials 10 (4) (2017) 437.
[7] T. Nagase, T. Sanda, A. Nino, W. Qin, H. Yasuda, H. Mori, Y. Umakoshi, J. A. Szpunar, J. Non-Cryst, Solids 358 (3) (2012) 502–518.
[8] T. Nagase, A. Takeuchi, K. Amiya, T. Egami, Mater. Chem. Phys. 210 (2018) 291–300.
[9] Y. Tong, S.J. Zhao, H.B. Bei, T. Egami, Y.W. Zhang, F.X. Zhang, Acta Materialia 183 (2020) 172–181.
[10] W. Guo, T. Iwashita, T. Egami, Acta Materialia 68 (2014) 229–237.
[11] Y.L. Chen, Y.H. Hu, C.W. Tsai, C.A. Hsieh, S.W. Kao, J.W. Yeh, T.S. Chin, S.K. Chen, J. Alloy. Compd. 477 (1–2) (2009) 696–705.
[12] T. Nagase, P.D. Rack, J.H. Noh, T. Egami, Intermetallics 59 (2015) 32–42.
[13] A.T. Motta, J. Nuclear Mater. 244 (3) (1997) 227–250.